ADVANCED OPTICAL MATERIALS
www.advopticalmat.de

www.MaterialsViews.com

Organic Heptamethine Salts for Photovoltaics and Detectors with Near-Infrared Photoresponse up to 1600 nm

*Margaret Young, John Suddard-Bangsund, Tyler J. Patrick, Natalia Pajares, Christopher J. Traverse, Miles C. Barr, Sophia Y. Lunt, and Richard R. Lunt**

Few organic photovoltaics (OPVs) and organic photodetectors have demonstrated photoresponse past 900 nm, a previously underutilized spectral region for tandem solar cells, transparent solar cells, and infrared photodetectors. In this work, heptamethine salts with selective deep near-infrared (NIR) photoresponse are demonstrated with external quantum efficiencies (EQEs) cutoffs at $\lambda = 1400$ or 1600 nm. Anion exchange is shown to deepen frontier orbital levels with minimal changes in absorption properties, leading to decreases in dark current, increases in open-circuit voltage (approaching excitonic limits), and increases in specific detectivity. Balancing exciton binding energy and charge transfer efficiency is shown to be the key for enhancing the performance of very small bandgap NIR-absorbing devices. These organic salts represent a pathway to inexpensive infrared solar cells and detectors, expanding the catalog of existing donor materials for transparent and multijunction solar cells.

Organic semiconductors that absorb in the NIR, i.e., at $\lambda > 800$ nm, are promising for applications in broadband and transparent solar cells.[1,2] Organic compounds with NIR photovoltaic response have been demonstrated including cyanines,[3–7] carbon nanotubes,[8] and polymers.[9,10] However, EQEs in these studies have only extended to 1100 nm for $SnNcCl_2$ and 1450 nm for carbon nanotubes. Design strategies for redshifting the IR absorption of organic molecules have included increasing the conjugation[4,11] and modifying the ligand structures to affect aggregation, crystal structure, and intermolecular proximities. However, once molecules are designed and integrated into optoelectronic devices, their performance typically suffers from arbitrary energy level alignments, resulting in lower-than-ideal open-circuit voltages, low carrier mobilities and diffusion lengths, and limited absorbance past 1000 nm. In this work, we synthesize a new series of heptamethine salts[12] with the highest occupied molecular orbital (HOMO) levels that can be tuned by varying the anion electronegativity.[13] These organic salts are used in photovoltaic and photodetector cells to demonstrate photoresponse at deep NIR wavelengths and open-circuit voltages nearing their excitonic limit. Using optical modeling and open-circuit voltage tuning[14,15] we identify limiting factors for performance and strategies for performance enhancement.

Heptamethine salts 1 (1-Butyl-2-(2-3-2-(1-butyl-1H-benzo[cd]indol-2-ylidene)-ethylidene-2-diphenylamino-cyclopent-1-enyl-vinyl)-benzo[cd]indolium, $\lambda_{max} = 996$ nm) and 2 (1-Butyl-2-(2-3-2-(1-butyl-1H-benzo[cd]indol-2-ylidene)-ethylidene-2-phenyl-cyclopent-1-enyl-vinyl)-benzo[cd]indolium, $\lambda_{max} = 1024$ nm) coordinated with the counterions tetrafluoroborate (BF_4^-) and tetrakis(pentafluorophenyl)borate ($TPFB^-$) are shown in **Figure 1**a. We focus on these molecules for their absorption ranges that extend to 1400 and 1600 nm for cations 1 and 2, respectively, (Figure 1b). Figure 1c shows a summary of the m/z synthesis verification for the cation and anion masses. In previous studies, weakly coordinating anions like TPFB have been shown to modulate the frontier energy levels of organic cations used as donors in photovoltaic configurations, thereby increasing the open circuit voltage (V_{OC}) with little or no impact on the bandgap or absorption range.[13,16]

Solar cell devices with the structure indium tin oxide (ITO)/10 nm MoO_3/t nm salt/40 nm C_{60}/7.5 nm bathocuproine (BCP)/80 nm Ag were prepared using the four salts as a function of thickness (**Figure 2**a). Donor layers of each organic salt were spin-coated from *N,N*-dimethylformamide under nitrogen while other layers were thermally deposited in vacuum. The thickness for each salt was controlled by varying the solution concentration. For comparison purposes, the J–V and EQE for devices with similar salt thicknesses (12 ± 1 nm) are plotted in Figure 2b,c and average performance metrics are shown in **Table 1**. The fill factors (FF) for these devices, 0.3–0.5, are slightly lower than our previous demonstrations with larger bandgap organic salts due to decreased shunt resistances from the lower bandgap and series resistance from a potential interface barrier between the donor and MoO_3. The exchange of BF_4 for TPFB nearly doubles the V_{OC} from 0.13 to 0.33 V for cation 1 and 0.17 to 0.25 V for cation 2. This enhancement in

M. Young, J. Suddard-Bangsund,[+] T. J. Patrick, N. Pajares,[++] C. J. Traverse, Prof. R. R. Lunt
Department of Chemical Engineering and Materials Science
Michigan State University
East Lansing, MI 48824, USA
E-mail: rlunt@msu.edu

Dr. M. C. Barr
Ubiquitous Energy, Inc
Redwood City, CA 94063, USA

Prof. S. Y. Lunt
Department of Biochemistry and Molecular Biology
Michigan State University
East Lansing, MI 48824, USA

Prof. R. R. Lunt
Department of Physics and Astronomy
Michigan State University
East Lansing, MI 48824, USA

[+]Present address: Department of Chemical Engineering and Materials Science, University of Minnesota, Minneapolis, MN 55455, USA
[++]Present address: Department of Materials Science, Technical University of Madrid, UPM, Madrid, Spain

DOI: 10.1002/adom.201600102

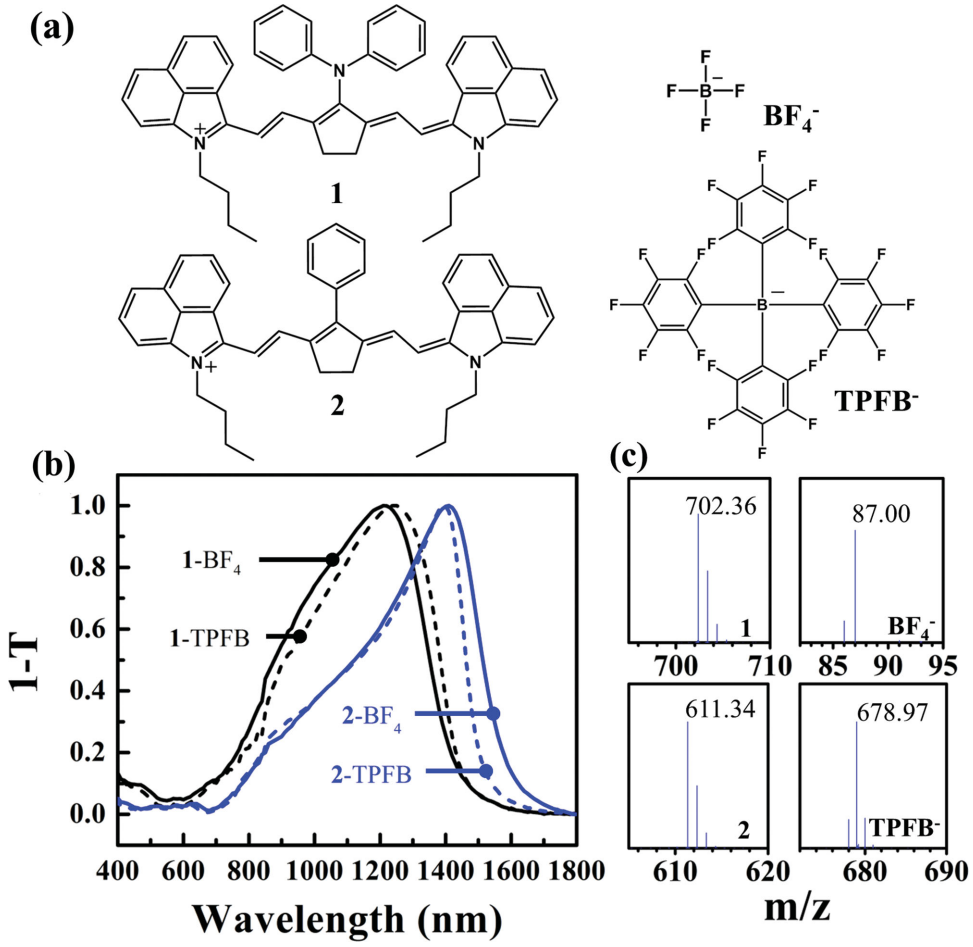

Figure 1. a) Chemical structures of the heptamethine salt cations (1 and 2) and anions (BF_4^- and tetraphenylfluoroborate, $TPFB^-$). b) Normalized thin film absorption (1-Transmission) of each organic salt. c) Summary of high-resolution mass spectrometry *m/z* spectra for cations and anions used in this study. The multiple peaks and their relative heights represent the isotopic abundances of the compound's constituent elements.

the voltage is due to the shift in frontier energy levels (see the Supporting Information for measured energy level schematic) and increased interface gap (**Figure 3**a). However, this exchange reduces the NIR EQE peak by more than 50% due to the substantial decrease in the donor–acceptor lowest unoccupied molecular orbital (LUMO) level offset (Δ_{LUMO}). To understand the effect of gradual shifts in interface gap on EQE, alloyed blends of 1- or 2-BF_4 with varying molar ratios of 1- or 2-TPFB were

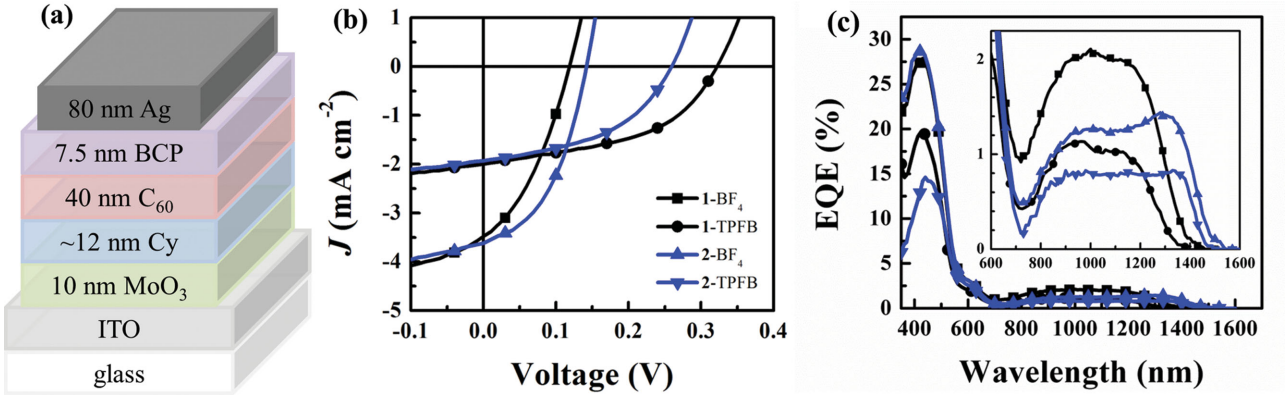

Figure 2. a) Device architecture used for photovoltaic and photodetector structures. b) Current density–voltage (*J–V*) and c) external quantum efficiency (EQE) curves for devices with salts with thicknesses of 12 nm (inset highlights the NIR EQE). The complete thickness dependent *J–V* data are provided in the Supporting Information.

Table 1. Device parameters and molecular properties for each salt.

Salt	J_{SC} [mA cm^{-2}]	V_{OC} [V]	FF	Abs. edge [nm]	NIR EQE peak [%]	D^* peak [Jones]	J_0 [μA cm^{-2}]
1-BF_4	3.4 ± 0.3	0.13 ± 0.01	0.34 ± 0.01	1440	2.1	3.7×10^9	48
1-TPFB	1.9 ± 0.2	0.33 ± 0.01	0.49 ± 0.01	1460	1.1	5.3×10^{10}	0.014
2-BF_4	3.4 ± 0.3	0.15 ± 0.01	0.42 ± 0.05	1590	1.4	7.0×10^9	7.0
2-TPFB	1.7 ± 0.2	0.25 ± 0.01	0.42 ± 0.04	1500	0.8	1.7×10^{10}	1.1

prepared. The V_{OC} and EQE trends as a function of TPFB molar fraction are plotted in **Figure 4**a.

The thickness trends of the pure salts are plotted in Figure 4b, where V_{OC} either remains flat (1-BF_4 and 2-BF_4) or decreases (1-TPFB and 2-TPFB) with increasing thickness and EQE monotonically increases. In general, the V_{OC} is found to be independent of donor salt thickness in the 5–15 nm range. In some cases, open-circuit voltages for OPVs increase with thickness as parallel shunting pathways are eliminated by the formation of more complete films.[17] In the case of 1- and 2-TPFB, however, V_{OC} shows a modest decrease of 20% over the thickness range of 4–15 nm. Decreases in V_{OC} with increasing thickness have previously been attributed to (1) increased recombination due to presence of disorder-induced gap tail states,[18] (2) increased recombination due to electric field profile broadening,[19] and (3) shifts in the interface gap due to band bending (Figure 3b).[20] Mechanisms (1) and (2) are unlikely due to the small thickness range (1 nm) over which the voltage drop occurs; thus, the V_{OC} decrease is most likely due to incomplete band bending in 1- and 2-TPFB devices as a function of thickness. In contrast, devices with 1- and 2-BF_4 have no thickness dependent photovoltage and therefore likely have smaller depletion widths stemming from either larger carrier densities or smaller dielectric constants.

Quantum efficiencies past 1000 nm have been limited in magnitude to <15% even for many quantum dot systems.[4,21] To identify the limiting factors in our NIR EQE, we examine the component efficiencies. EQE can be expressed as the product of the internal efficiencies: η_A (absorption), η_{ED} (exciton diffusion), η_{CT} (charge transfer), η_{CD} (charge dissociation), and η_{CC} (charge collection). Through exciton diffusion and optical interference modeling,[22,23] EQE curves were well fit for effective

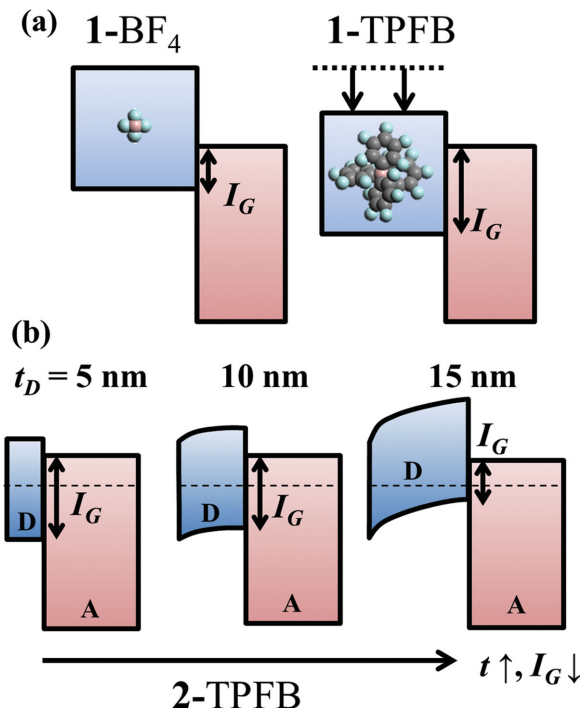

Figure 3. a) Energy schematic illustrating the deepening of the LUMO level and increase in interface gap (I_G) after counterion exchange from the small anion BF_4 to the bulky and weakly coordinating anion $TPFB^-$. b) Schematic donor-acceptor (D–A) band structure as a function of donor thickness (t_D).

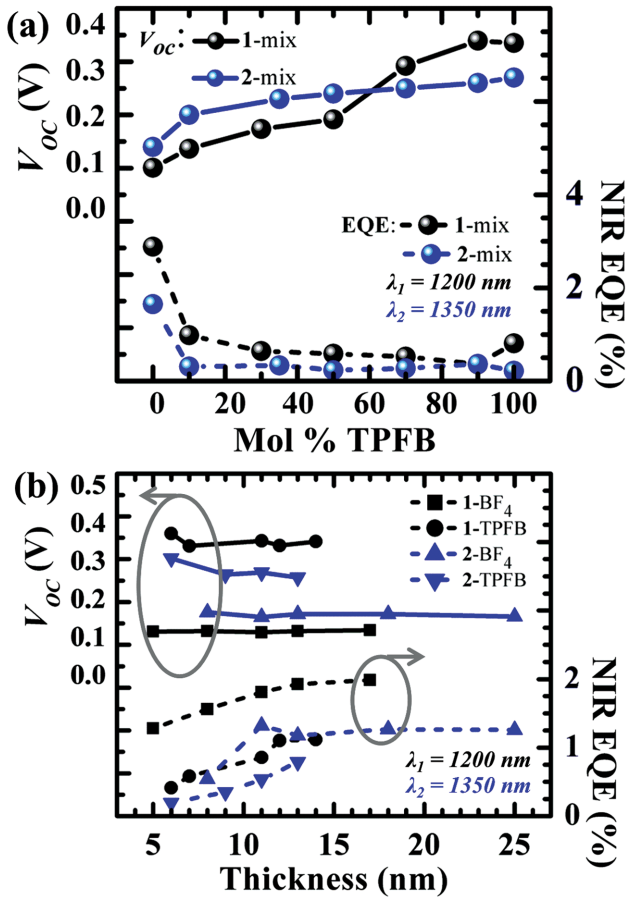

Figure 4. a) V_{OC} (left axis) and EQE (right axis) as functions of mole fraction TPFB for blends of (black) 1-BF_4 and 1-TPFB and (blue) 2-BF_4 and 2-TPFB at t_D= 6 nm. b) EQE and V_{OC} as a function of donor thickness. Wavelength of EQE is shown in inset: 1200 nm for 1-BF_4 and 1-TPFB and 1350 nm for 2-BF_4 and 2-TPFB.

exciton diffusion lengths, which were calculated assuming 100% charge transfer, charge dissociation, and charge collection efficiencies. From this analysis we find that the effective diffusion lengths in these four salts are all around 0.5–1 nm due to the modest EQEs. However, we also find that absorption profiles already reach 70% at the peak wavelength for 2-TPFB films that are only 25 nm thick, suggesting that these devices are not limited by absorption. With the extracted diffusion lengths, the optical interference model predicts that the EQE should decrease for all the tested salts with increasing thickness due to the inability of excitons to diffuse to the dissociating interface. This predicted trend of decreasing EQE is indeed seen experimentally in other larger gap cyanine salt devices.[13,19] However, this behavior is in contrast to the experimental trends here, which show EQE monotonically increasing for donor layer thicknesses past 25 nm. This suggests that the intrinsic diffusion length is in fact longer than 0.5–1 nm and the EQE of these salts is instead limited by charge transfer, charge dissociation, or charge collection efficiency, at least one of which should not be modeled as 100%.

While there is not a clear method to directly distinguish among all of these component efficiencies (charge transfer, dissociation, and collection), we can infer insight about charge collection from other measurements. For example, since the experimental C_{60} EQE peak (λ = 430 nm) does not decrease with increasing salt thickness and is similar in magnitude to other salt based OPVs with larger bandgaps,[7,13] this implies that hole collection from excitons originating on C_{60} (which still have to transport through the donor salt) is not a limiting factor. Thus, devices are most likely limited by charge transfer or dissociation efficiency as a result of the balance between the lowest unoccupied molecular orbitals of the donor and acceptor and the exciton binding energy.

To estimate the exciton binding energy, we turn to anion mixing experiments and look for the emergence of sharp cutoffs in the EQE (Figure 4a). Indeed, while there is a linear variation in the V_{OC} that stems from a monotonic modulation of interface gap recombination, there is a sharp EQE cutoff at a molar fraction of 10% TPFB, suggesting that there is just enough energy (Δ_{LUMO}) available at that concentration to efficiently overcome the exciton binding energy. The remaining quantum efficiency beyond this concentration likely stems from a combination of field- and temperature-driven dissociation.[24] We can then estimate the energy available for exciton dissociation by subtracting the interface gap (calculated from the V_{OC})[25] from the optical bandgap, yielding exciton binding energies of ≈0.55 eV for 1 and ≈0.40 eV for 2, which is close to other reported values in organic molecules (0.2–1.4 eV).[26–28] These exciton binding energies make up roughly 50% of the optical bandgap (≈0.8 eV), limiting the interface gap (and therefore V_{OC}) to modest values at which efficient exciton dissociation can still take place, despite the ability to achieve higher V_{OC} values. Moving forward, several strategies can be explored to decrease the exciton binding energy. For example, molecular modifications can be designed to enhance the delocalization of the electron/hole orbitals to increase the exciton radius,[29] e.g., via central methine subsitution.[12] Another design strategy involves the coupling of denser solubilizing groups or anions that allow for greater packing to increase the dielectric

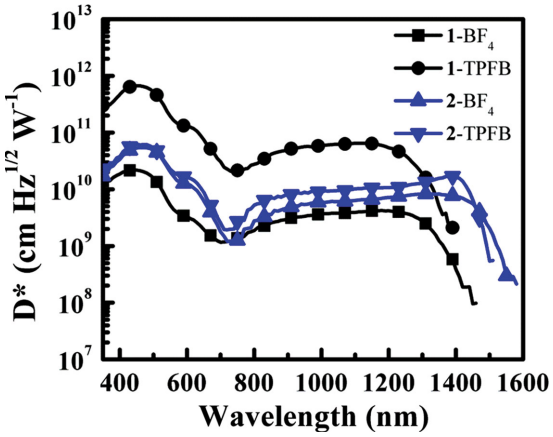

Figure 5. Specific detectivity *D** spectra for devices made with each salt donor.

constant.[27,30,31] Thus, this presents an interesting design challenge for the future optimization of very small bandgap organic photoactive devices.

To understand the ultimate potential of these material sets in photovoltaic applications, we modeled the EQE of a device with a 100 nm thick 2-TPFB layer having an exciton diffusion length of 100 nm, a 20 nm thick C_{60} layer, and charge transfer and charge collection efficiencies approaching 100%. Such a device would have an EQE of about 70%–80% with a J_{SC} on the order of 25 mA cm^{-2} and could be realized using a bulk heterojunction architecture and optimized energy level tuning. FF values can be increased from 0.3 to 0.65 (achievable for many organic systems) by optimizing the interface energetics or the modification of solvent processing conditions. Combined with a slightly improved V_{OC} of 0.55 V, which is around the Shockley–Queisser excitonic limit, ideal devices would be 10% efficient with high transparency and would be well suited for multijunction cells with complimentary absorption.

These salt-based devices are also shown to be viable for near infrared photodetectors.[32] Photodetector devices were fabricated with the same photovoltaic structure as those above. Specific detectivity (*D**) curves for each salt are plotted in **Figure 5**, where *D** is proportional to the EQE and inversely proportional to the differential resistance at zero bias (see the Supporting Information).[33] Calculated *D** values are comparable to those of the limited reports in other organic systems[11,33–35] and reach values of 6.5×10^{10} Jones at λ = 1140 nm and 1.7×10^{10} Jones at λ = 1390 nm for 1- and 2- salts, respectively. This compares well to the very limited reports in organic systems, such as porphyrin tapes (2.3×10^{10} Jones at λ = 1350 nm)[11] and inorganic carbon nanotubes (8.8×10^{11} Jones at λ = 1350 nm).[33] Exchanging the anion from 1-BF_4 to 1-TPFB increases the detectivity by an order of magnitude from 3.7×10^9 to 5.3×10^{10} Jones, largely due to lower noise currents for devices with the TPFB anion (Figure S4, Supporting Information). Compared to other organic systems, heptamethine salts have readily tunable properties via counterion or ligand exchange in addition to being easy to synthesize and fabricate. Moreover, they exhibit both broader and wavelength-specific photoresponsivity, which is promising for a range of applications in the near-infrared including visibly transparent photodetectors.

In summary, we have demonstrated simple organic salts with unusually low bandgaps (0.8 eV) for infrared photoresponsivity extending to 1 600 nm. These salts are demonstrated in both photovoltaics and photodetectors and obtain peak NIR EQEs approaching 5% with standard fullerene acceptors. Performing counterion exchanges on these heptamethine salts is shown to increase the interface gap – along with V_{OC}, dark saturation current, and D^* – with an eventual tradeoff in the exciton dissociation and quantum efficiency due to the modest exciton binding energies (≈0.4–0.55 eV). Nonetheless, anion exchange and alloying allow for facile tuning of the interface gap and provide interesting insight into the binding energies of these very small bandgap salts. The optimization of these heptamethine salts represents a promising new approach to extend the range of NIR photoresponsive devices and enables new routes to the development of low cost infrared detectors and high efficiency multijunction cells.

Experimental Section

Synthesis of 1-TPFB and 2-TPFB: Equimolar amounts of potassium tetrakis(pentaflurophenyl)borate (K-TPFB) and either 1- or 2-BF_4 were dissolved in 5:1 methanol:dichloromethane (MeOH:DCM) at 10 mg mL^{-1} and stirred at room temperature under nitrogen for 1 h prior to reaction. All chemicals were used as received (Boulder Scientific Company, Few), and solvents were high-performance liquid chromatography (HPLC) grade (Sigma-Aldrich). The solid product was collected using vacuum filtration and an MeOH wash, redissolved in minimal DCM (≈10 mg mL^{-1}), and poured through a plug of silica using DCM as eluent to remove impurities and unreacted 1- or 2-BF_4. The first fraction with similar color to 1- or 2-BF_4 was collected, and excess DCM was removed in a rotary evaporator at 55 °C for 20 min at atmospheric pressure.

Verification of 1-TPFB and 2-TPFB and Ion Purity Assessment: Verification of cations, anions, and product purity were performed using a Waters Xevo G2-XS QToF mass spectrometer coupled to a Waters Acquity ultrahigh pressure liquid chromatography (LC) system. Cations were analyzed in positive ion mode electrospray ionization (ESI), and anions were analyzed in negative ion mode ESI. Solutions were prepared in acetonitrile and directly injected for 2 min using an eluent of 50:50 water:acetonitrile. Mass spectra were acquired using a dynamic range extension over m/z 50–1500, with mass resolution ($M/\Delta M$, full width-half maximum) of ≈20 000. Other parameters included capillary voltage of 2 kV, desolvation temperature of 350 °C, source temperature of 100 °C, cone gas (N_2) at 0 L h^{-1}, and desolvation gas (N_2) at 400 L h^{-1}. The m/z calculated for cation 1 in 1-TPFB ($C_{51}H_{48}N_3^+$) is 702.3848, and the measured m/z is 702.3641. The m/z calculated for TPFB$^-$ anion in 1-TPFB ($C_{24}BF_{20}^-$) is 678.9774, and the measured m/z is 678.9788. The m/z calculated for cation 2 in 2-TPFB ($C_{45}H_{43}N_2^+$) is 611.3426, and the measured m/z is 611.3421. The m/z calculated for TPFB$^-$ anion in 2-TPFB ($C_{24}BF_{20}^-$) is 678.9774, and the measured m/z is 678.9789.

For ion purity assessment, solutions of the exchange precursors and products were prepared in acetonitrile with concentrations varying from 10×10^{-9} to 500×10^{-9} M and analyzed by mass spectrometry as described above. Calibration curves of integrated ion detection intensity for precursors K-TPFB, 1-BF_4, and 2-BF_4 versus concentration were calculated to measure BF_4^- and TPFB$^-$ ion concentrations in the exchange products 1-TPFB and 2-TPFB. The ion purity was measured to be >95% TPFB for both 1-TPFB and 2-TPFB.

Solar Cell Device Fabrication and Testing: Patterned ITO substrates (Xin Yan, 100 nm, 20 Ω sq^{-1}) were sequentially cleaned in soap, deionized water, acetone, and boiling isopropanol for 3 min each. Substrates were then oxygen plasma treated for 3 min, and MoO_3 (99.9995%, Alfa Aesar) was thermally evaporated at 0.1 nm s^{-1} at 3×10^{-6} torr. Heptamethine salts were massed in air, dissolved in dimethyl formamide under a nitrogen environment, and sonicated for at least 30 min. Solutions were used without filtering and spincoated at 3000 rpm for 30 s in a glovebox. Subsequent layers of C_{60} (99.9%, MER Corp.), BCP (Luminescence Technology, Inc.), and silver were thermally evaporated at 0.1, 0.05, and 0.2 nm s^{-1}, respectively. Layer thicknesses were measured using variable-angle spectroscopic ellipsometry (J. A. Woollam) on Si substrates. Device areas (average value: 5.7 mm^2) were defined as the area of overlap between the anode and cathode and were measured using optical microscopy. Current density (J) was measured as a function of voltage using a Labview-controlled sourcemeter under xenon arc lamp illumination calibrated for AM1.5G (100 mW mm^{-2}) intensity using a NREL-calibrated Si reference cell with KG5 filter. EQE measurements were performed by using monochromatic light from a tungsten halogen lamp chopped at 200 Hz, a picoammeter, and a lock-in amplifier. The light intensity at the end of the IR-fiber was measured using a Newport calibrated Si diode for 350–800 nm and a Newport calibrated Ge diode for 800–1600 nm. Specific detectivity D^* (cm Hz$^{1/2}$ W^{-1}) was calculated based on J–V measurements at short circuit ($V = 0$). D^* was obtained from

$$D^* = R\sqrt{A}S_N^{-1} \quad (1)$$

where R is responsivity in A W^{-1}, A is device area in cm^2, and S_N^{-1} is current spectral noise density in A Hz$^{-1/2}$. At room temperature and 0 V, the noise was dominated by thermal (Johnson–Nyquist) noise S_T (A Hz$^{-1/2}$), which was estimated as

$$S_T = \sqrt{\frac{4k_BT}{R_D}} \quad (2)$$

where k_B is the Boltzmann constant (J K^{-1}), T is temperature (K), and R_D is the differential resistance of the device in the dark at zero bias.

Ultraviolet photoelectron spectroscopy data were recorded with a He lamp emitting at 21.2 eV (He I radiation) on 10 nm thick salt films on MoO_3/ITO. The samples were loaded without exposure to air. LUMO transport levels were estimated by adding the optical bandgaps (0.85 eV for 1-BF_4 and 1-TPFB and 0.80 eV for 2-BF_4 and 2-TPFB) and calculated exciton binding energies (0.55 eV for 1-BF_4 and 1-TPFB and 0.40 eV for 2-BF_4 and 2-TPFB) to the HOMO levels.

Supporting Information

Supporting Information is available from the Wiley Online Library or from the author.

Acknowledgements

Financial support for this work was provided by the National Science Foundation (CAREER award (CBET-1254662) and (IIP-1431010)), and a DuPont Young Professor Award. Support was also provided by the Department of Education through a Graduate Assistantship in Areas of National Need Award (GAANN, Award GU0115873). The authors would like to thank the MSU Mass Spectrometry Core for access to the mass spectrometry facilities.

Received: February 19, 2016
Revised: March 15, 2016
Published online: April 15, 2016

[1] R. R. Lunt, V. Bulovic, *Appl. Phys. Lett.* **2011**, *98*, 113305.
[2] C.-C. Chen, L. Dou, R. Zhu, C.-H. Chung, T.-B. Song, Y. B. Zheng, S. Hawks, G. Li, P. S. Weiss, Y. Yang, *ACS Nano* **2012**, *6*, 7185.
[3] B. P. Rand, J. Xue, F. Yang, S. R. Forrest, *Appl. Phys. Lett.* **2005**, *87*, 233508.

[4] R. Pandey, R. A. Kerner, S. M. Menke, J. Holst, K. V. B. Josyula, R. J. Holmes, *Org. Electron.* **2013**, *14*, 804.
[5] M. Hiramoto, K. Kitada, K. Iketaki, T. Kaji, *Appl. Phys. Lett.* **2011**, *98*, 023302.
[6] H.-S. Shim, H. J. Kim, J. W. Kim, S.-Y. Kim, W.-I. Jeong, T.-M. Kim, J.-J. Kim, *J. Mater. Chem.* **2012**, *22*, 9077.
[7] A. C. Véron, H. Zhang, A. Linden, F. Nüesch, J. Heier, R. Hany, T. Geiger, *Org. Lett.* **2014**, *16*, 1044.
[8] M. J. Shea, M. S. Arnold, *Appl. Phys. Lett.* **2013**, *102*, 243101.
[9] Y. Xia, L. Wang, X. Deng, D. Li, X. Zhu, Y. Cao, *Appl. Phys. Lett.* **2006**, *89*, 081106.
[10] L. Dou, Y. Liu, Z. Hong, G. Li, Y. Yang, *Chem. Rev.* **2015**, *115*, 12633.
[11] J. D. Zimmerman, V. V. Diev, K. Hanson, R. R. Lunt, E. K. Yu, M. E. Thompson, S. R. Forrest, *Adv. Mater.* **2010**, *22*, 2780.
[12] C. A. Bertolino, G. Caputo, C. Barolo, G. Viscardi, S. Coluccia, *J. Fluoresc.* **2006**, *16*, 221.
[13] J. Suddard-Bangsund, C. J. Traverse, M. Young, T. J. Patrick, Y. Zhao, R. R. Lunt, *Adv. Energy Mater.* **2016**, *6*, 1501659.
[14] P. P. Khlyabich, B. Burkhart, B. C. Thompson, *J. Am. Chem. Soc.* **2011**, *133*, 14534.
[15] P. P. Khlyabich, A. E. Rudenko, B. C. Thompson, Y.-L. Loo, *Adv. Funct. Mater.* **2015**, *25*, 5557.
[16] P.-A. Bouit, C. Aronica, L. Toupet, B. Le Guennic, C. Andraud, O. Maury, *J. Am. Chem. Soc.* **2010**, *132*, 4328.
[17] T. P. Osedach, A. Iacchetti, R. R. Lunt, T. L. Andrew, P. R. Brown, G. M. Akselrod, V. Bulović, *Appl. Phys. Lett.* **2012**, *101*, 113303.
[18] J. C. Blakesley, D. Neher, *Phys. Rev. B* **2011**, *84*, 075210.
[19] S. Jenatsch, T. Geiger, J. Heier, C. Kirsch, F. Nüesch, A. Paracchino, D. Rentsch, B. Ruhstaller, A. C Véron, R. Hany, *Sci. Technol. Adv. Mater.* **2015**, *16*, 035003.
[20] A. Kahn, N. Koch, W. Gao, *J. Polym. Sci., Part B Polym. Phys.* **2003**, *41*, 2529.
[21] P. R. Brown, R. R. Lunt, N. Zhao, T. P. Osedach, D. D. Wanger, L.-Y. Chang, M. G. Bawendi, V. Bulović, *Nano Lett.* **2011**, *11*, 2955.
[22] P. Peumans, A. Yakimov, S. R. Forrest, *J. Appl. Phys.* **2003**, *93*, 3693.
[23] M. Young, C. J. Traverse, R. Pandey, M. C. Barr, R. R. Lunt, *Appl. Phys. Lett.* **2013**, *103*, 133304.
[24] P. Peumans, S. R. Forrest, *Chem. Phys. Lett.* **2004**, *398*, 27.
[25] R. R. Lunt, T. P. Osedach, P. R. Brown, J. A. Rowehl, V. Bulović, *Adv. Mater.* **2011**, *23*, 5712.
[26] I. G. Hill, A. Kahn, Z. G. Soos, J. R. A. Pascal, *Chem. Phys. Lett.* **2000**, *327*, 181.
[27] S. Kraner, R. Scholz, C. Koerner, K. Leo, *J. Phys. Chem. C* **2015**, *119*, 22820.
[28] A. Dkhissi, *Synth. Met.* **2011**, *161*, 1441.
[29] M. Knupfer, *Appl. Phys. A: Mater. Sci. Process.* **2003**, *77*, 623.
[30] N. Cho, C. W. Schlenker, K. M. Knesting, P. Koelsch, H.-L. Yip, D. S. Ginger, A. K.-Y. Jen, *Adv. Energy Mater.* **2014**, *4*, 1301857.
[31] S. Kraner, C. Koerner, K. Leo, E. Bittrich, K.-J. Eichhorn, Y. Karpov, A. Kiriy, M. Stamm, K. Hinrichs, M. Al-Hussein, *Phys. Rev. B* **2015**, *91*, 195202.
[32] H. Zhang, S. Jenatsch, J. De Jonghe, F. Nüesch, R. Steim, A. C. Véron, R. Hany, *Sci. Rep.* **2015**, *5*, 9439.
[33] M. S. Arnold, J. D. Zimmerman, C. K. Renshaw, X. Xu, R. R. Lunt, C. M. Austin, S. R. Forrest, *Nano Lett.* **2009**, *9*, 3354.
[34] Y. Xie, M. Gong, T. A. Shastry, J. Lohrman, M. C. Hersam, S. Ren, *Adv. Mater.* **2013**, *25*, 3433.
[35] Z. Su, F. Hou, X. Wang, Y. Gao, F. Jin, G. Zhang, Y. Li, L. Zhang, B. Chu, W. Li, *ACS Appl. Mater. Interfaces* **2015**, *7*, 2529.